Electronic Supplementary Material (ESI) for Physical Chemistry Chemical Physics.

Supporting information for:

σ Bond Activation Through Tunneling: Formation of the Boron Hydride Cations BH_n^+ (n = 2, 4, 6)

Yudong Qiu, Chia-Hua Wu, Henry F. Schaefer III, Wesley D. Allen,* and Jay Agarwal*

Center for Computational Quantum Chemistry

University of Georgia

Athens, Georgia 30602

E-mail: wdallen@uga.edu; jagarwal@uga.edu

Contents

1 Optimized Structures

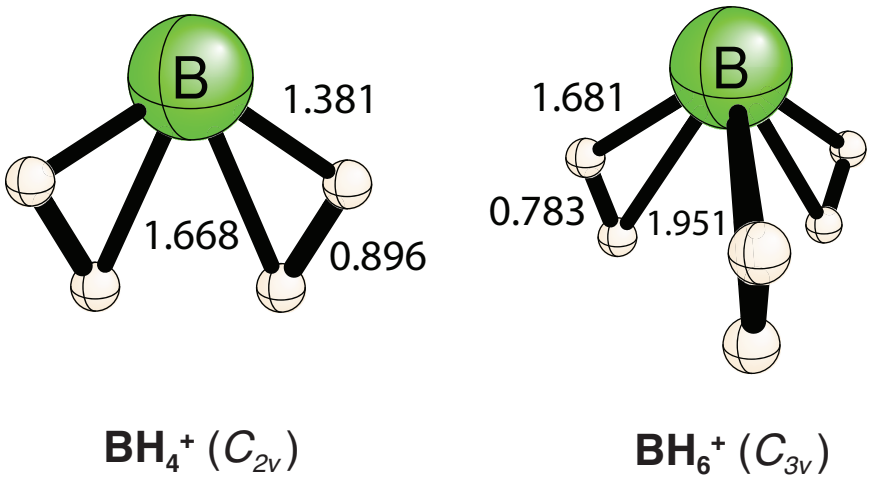

Figure S1: Optimized distances (Å) for the insertion transition states of BH_4^+ (C_{2v}) and BH_6^+ (C_{3v}) at the CCSD(T)/cc-pCV5Z level of theory.

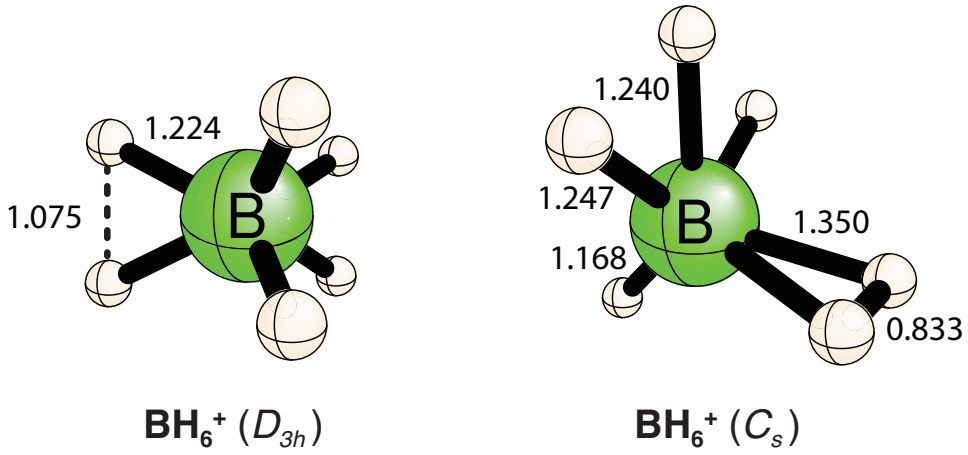

Figure S2: Optimized distances (Å) for the hydrogen scrambling transition states at the CCSD(T)/cc-pCV5Z level of theory.

Table S1: Optimized Cartesian coordinates (Å) of $B(H_2)^+$ at CCSD(T)/cc-pCV5Z level of theory.

Atoms	X	Y	Z
B	0.000 00	0.000 00	−0.345 00
H	0.000 00	−0.377 83	1.884 36
H	0.000 00	0.377 83	1.884 36

Table S2: Optimized Cartesian coordinates (Å) of $B(H_2)_2^+$ at CCSD(T)/cc-pCV5Z level of theory.

Atoms	X	Y	Z
B	0.431 93	0.166 06	0.000 00
H	−1.711 31	0.865 90	0.377 25
H	−1.711 31	0.865 90	−0.377 25
H	−0.313 16	−1.947 83	0.000 00
H	−0.982 55	−1.598 01	0.000 00

Table S3: Optimized Cartesian coordinates (Å) of $B(H_2)_3^+$ at CCSD(T)/cc-pCV5Z level of theory.

Atoms	X	Y	Z
B	0.000 00	0.000 00	−0.542 26
H	1.825 14	0.000 00	0.774 36
H	−0.912 57	1.580 62	0.774 36
H	−0.912 57	−1.580 62	0.774 36
H	1.394 59	0.450 64	1.200 14
H	−1.087 57	0.982 43	1.200 14
H	−0.307 03	−1.433 07	1.200 14

Table S4: Optimized Cartesian coordinates (Å) of HBH^+ at CCSD(T)/cc-pCV5Z level of theory.

Atoms	X	Y	Z
B	0.000 00	0.000 00	0.000 00
H	0.000 00	0.000 00	−1.170 58
H	0.000 00	0.000 00	1.170 58

Table S5: Optimized Cartesian coordinates (Å) of $HBH(H_2)^+$ at CCSD(T)/cc-pCV5Z level of theory.

Atoms	X	Y	Z
B	0.000 00	0.000 00	0.129 91
H	1.105 16	0.000 00	0.522 46
H	−1.105 16	0.000 00	0.522 46
H	−0.407 80	0.000 00	−1.232 03
H	0.407 80	0.000 00	−1.232 03

Table S6: Optimized Cartesian coordinates (Å) of $HBH(H_2)_2^+$ at CCSD(T)/cc-pCV5Z level of theory.

Atoms	X	Y	Z
B	0.000 00	0.000 00	−0.130 77
H	−1.035 01	0.000 00	−0.698 84
H	1.035 01	0.000 00	−0.698 84
H	0.411 66	1.004 65	0.706 54
H	−0.411 66	1.004 65	0.706 54
H	−0.411 66	−1.004 65	0.706 54
H	0.411 66	−1.004 65	0.706 54

Table S7: Optimized Cartesian coordinates (Å) of $B(H_2)_2^+$ insertion TS with C_{2v} symmetry at CCSD(T)/cc-pCV5Z level of theory.

Atoms	X	Y	Z
B	0.000 00	0.000 00	−0.306 86
H	0.000 00	−1.150 03	0.457 88
H	0.000 00	1.150 03	0.457 88
H	0.000 00	−0.675 65	1.218 19
H	0.000 00	0.675 65	1.218 19

Table S8: Optimized Cartesian coordinates (Å) of $B(H_2)_3^+$ insertion TS with C_{3v} symmetry at CCSD(T)/cc-pCV5Z level of theory.

Atoms	X	Y	Z
B	−0.434 50	0.000 00	0.000 00
H	0.430 45	−0.720 47	−1.247 89
H	0.430 45	1.440 94	0.000 00
H	0.430 45	−0.720 47	1.247 89
H	1.151 69	−0.568 04	−0.983 87
H	1.151 69	1.136 07	0.000 00
H	1.151 69	−0.568 04	0.983 87

Table S9: Optimized Cartesian coordinates (Å) of $HBH(H_2)_2^+$ hydrogen scrambling TS with D_{3h} symmetry at CCSD(T)/cc-pCV5Z level of theory.

Atoms	X	Y	Z
B	0.000 00	0.000 00	0.000 00
H	−0.952 65	−0.537 71	−0.550 01
H	−0.952 65	0.537 71	−0.550 01
H	0.000 00	0.537 71	1.100 02
H	0.000 00	−0.537 71	1.100 02
H	0.952 65	−0.537 71	−0.550 01
H	0.952 65	0.537 71	−0.550 01

Table S10: Optimized Cartesian coordinates (Å) of $HBH(H_2)_2^+$ hydrogen scrambling TS with C_s symmetry at CCSD(T)/cc-pCV5Z level of theory.

Atoms	X	Y	Z
B	0.033 31	−0.113 32	0.000 00
H	0.185 40	−1.271 85	0.000 00
H	0.787 86	0.871 08	0.000 00
H	−1.157 36	0.367 59	−0.416 38
H	−1.157 36	0.367 59	0.416 38
H	0.488 78	0.451 75	−1.014 37
H	0.488 78	0.451 75	1.014 37

2 Focal Point Analyses

Table S11: Focal point analysis for the energies of the stationary points on the BH_2^+ PES relative to the reactant $B(H_2)^+$ (ΔE, kcal mol^{-1}).[a]

Basis Set	ΔE_e[CAS(2,2)]	δ[Mk-MRPT2[b]]	δ[Mk-MRCCSD]	δ[Mk-MRCCSD(T)]	ΔE_e[Mk-MRCCSD(T)]
(a) $B(H_2)^+ \rightarrow$ TS					
cc-pCVDZ	+48.18	+8.71	+8.51	−1.90	[+63.50]
cc-pCVTZ	+48.35	+8.81	+7.77	−2.24	[+62.69]
cc-pCVQZ	+48.32	+8.50	+7.57	−2.34	[+62.06]
cc-pCV5Z	+48.28	+8.48	+7.50	−2.36	[+61.89]
cc-pCV6Z	+48.27	+8.47	+7.47	−2.37	[+61.83]
CBS limit	[+48.27]	[+8.45]	[+7.43]	[−2.38]	[+61.76]
ΔE = 61.76 − 3.42 = +58.34 kcal mol^{-1}					
(b) $B(H_2)^+ \rightarrow HBH^+$					
cc-pCVDZ	−55.27	−3.03	+5.93	+0.09	[−52.28]
cc-pCVTZ	−55.90	−6.44	+5.22	+0.14	[−56.98]
cc-pCVQZ	−55.90	−7.80	+5.29	+0.19	[−58.22]
cc-pCV5Z	−55.91	−8.22	+5.40	+0.21	[−58.52]
cc-pCV6Z	−55.91	−8.41	+5.46	+0.22	[−58.64]
CBS limit	[−55.91]	[−8.68]	[+5.55]	[+0.22]	[−58.81]
ΔE = -58.81 + 3.65 = −55.16 kcal mol^{-1}					

[a]Geometries used in this table were optimized at FCI/cc-pVTZ level of theory. The symbol δ denotes the increment in the relative energy with respect to the preceding level of theory in the hierarchy CASSCF→Mk-MRPT2→Mk-MRCCSD→Mk-MRCCSD(T). Square brackets signify results obtained from basis set extrapolations. Each final relative energy ΔE is the sum of ΔE_e[Mk-MRCCSD(T)/CBS] and Δ_{ZPVE}[FCI/cc-pVTZ], listed in order.
[b]Evangelista, F. A.; Simmonett. A. C.; Schaefer, H. F. *Phys. Chem. Chem. Phys.* **2009**, 11(23), 4728-4741.

Table S12: Focal point analysis for the energies of the stationary points on the BH_4^+ PES relative to the reactant $B(H_2)_2^+$ (ΔE, kcal mol^{-1}).[a]

Basis Set	ΔE_e[HF]	δ[MP2]	δ[CCSD]	δ[CCSD(T)]	δ[CCSDT]	δ[CCSDT(Q)]	δ[CCSDTQ]	ΔE_e[CCSDTQ]
(a) $B(H_2)_2^+ \rightarrow$ TS								
cc-pCVDZ	+25.28	−15.39	+5.01	−2.24	−0.43	−0.12	−0.02	[+12.09]
cc-pCVTZ	+26.56	−17.10	+4.90	−2.74	−0.38	−0.15	[−0.02]	[+11.07]
cc-pCVQZ	+26.65	−17.91	+4.93	−2.84	−0.35	[−0.15]	[−0.02]	[+10.31]
cc-pCV5Z	+26.65	−18.08	+4.96	−2.86	[−0.35]	[−0.15]	[−0.02]	[+10.14]
cc-pCV6Z	+26.65	−18.18	+4.99	−2.87	[−0.35]	[−0.15]	[−0.02]	[+10.06]
CBS limit	[+26.65]	[−18.33]	[+5.03]	[−2.88]	[−0.35]	[−0.15]	[−0.02]	[+9.94]
ΔE = 9.94 + 2.19 + 0.02 + 0.05 = +12.20 kcal mol^{-1}								
(b) $B(H_2)_2^+ \rightarrow HBH(H_2)^+$								
cc-pCVDZ	−75.43	−1.12	+10.01	−0.29	−0.08	+0.00	+0.00	[−66.91]
cc-pCVTZ	−75.91	−4.62	+8.70	−0.41	−0.07	+0.01	[+0.00]	[−72.30]
cc-pCVQZ	−75.99	−6.03	+8.55	−0.39	−0.06	[+0.01]	[+0.00]	[−73.91]
cc-pCV5Z	−76.03	−6.39	+8.57	−0.38	[−0.06]	[+0.01]	[+0.00]	[−74.28]
cc-pCV6Z	−76.03	−6.56	+8.59	−0.37	[−0.06]	[+0.01]	[+0.00]	[−74.43]
CBS limit	[−76.03]	[−6.81]	[+8.62]	[−0.37]	[−0.06]	[+0.01]	[+0.00]	[−74.63]
ΔE = -74.63 + 7.50 − 0.03 + 0.11 = −67.05 kcal mol^{-1}								

[a]The symbol δ denotes the increment in the relative energy with respect to the preceding level of theory in the hierarchy HF→MP2→CCSD→CCSD(T)→CCSDT→CCSDT(Q)→CCSDTQ.
Square brackets signify results obtained from basis set extrapolations or additivity assumptions.
[b]Each final relative energy ΔE is the sum of ΔE_e[CCSDTQ/CBS], Δ_{ZPVE}[CCSD(T)/cc-pCVQZ], Δ_{DBOC}[CCSD/cc-pCVQZ], and Δ_{rel}[CCSD(T)/cc-pCVQZ], listed in order.

Table S13: Focal point analysis for the energies of the stationary points on the BH_6^+ PES (ΔE, kcal mol^{-1}).[a]

Basis Set	ΔE_e[HF]	δ[MP2]	δ[CCSD]	δ[CCSD(T)]	δ[CCSDT]	δ[CCSDT(Q)]	δ[CCSDTQ]	ΔE_e[CCSDTQ]
(a) $B(H_2)_3^+ \rightarrow C_{3v}$ insertion TS								
cc-pCVDZ	+12.92	−10.17	+3.18	−1.62	−0.30	−0.06	−0.01	[+3.92]
cc-pCVTZ	+13.79	−11.70	+3.16	−2.06	−0.29	−0.10	[−0.01]	[+2.79]
cc-pCVQZ	+13.92	−12.18	+3.18	−2.15	−0.27	[−0.10]	[−0.01]	[+2.39]
cc-pCV5Z	+13.92	−12.31	+3.20	−2.17	[−0.27]	[−0.10]	[−0.01]	[+2.27]
cc-pCV6Z	+13.92	−12.38	+3.22	−2.18	[−0.27]	[−0.10]	[−0.01]	[+2.21]
CBS limit	[+13.92]	[−12.49]	[+3.25]	[−2.19]	[−0.27]	[−0.10]	[−0.01]	[+2.12]
$\Delta E = 2.12 + 2.42 - 0.01 + 0.03 = +4.55$ kcal mol^{-1}								
(b) $B(H_2)_3^+ \rightarrow HBH(H_2)_2^+$								
cc-pCVDZ	−84.20	−10.63	+11.14	−0.88	−0.10	−0.01	+0.00	[−84.69]
cc-pCVTZ	−84.82	−15.42	+10.03	−1.32	−0.08	−0.01	[+0.00]	[−91.61]
cc-pCVQZ	−84.87	−17.24	+9.89	−1.36	−0.06	[−0.01]	[+0.00]	[−93.65]
cc-pCV5Z	−84.91	−17.66	+9.91	−1.36	[−0.06]	[−0.01]	[+0.00]	[−94.08]
cc-pCV6Z	−84.91	−17.87	+9.94	−1.36	[−0.06]	[−0.01]	[+0.00]	[−94.26]
CBS limit	[−84.91]	[−18.16]	[+9.98]	[−1.35]	[−0.06]	[−0.01]	[+0.00]	[−94.52]
$\Delta E = -94.52 + 12.13 - 0.11 + 0.14 = -82.36$ kcal mol^{-1}								
(c) $HBH(H_2)_2^+ \rightarrow D_{3h}$ scrambling TS								
cc-pCVDZ	+34.90	−12.13	+2.27	−1.05	−0.09	−0.09	−0.01	[+23.81]
cc-pCVTZ	+35.30	−13.55	+2.70	−1.43	−0.05	−0.11	[−0.01]	[+22.86]
cc-pCVQZ	+35.38	−13.99	+2.79	−1.51	−0.03	[−0.11]	[−0.01]	[+22.53]
cc-pCV5Z	+35.39	−14.09	+2.82	−1.53	[−0.03]	[−0.11]	[−0.01]	[+22.44]
cc-pCV6Z	+35.39	−14.14	+2.84	−1.54	[−0.03]	[−0.11]	[−0.01]	[+22.40]
CBS limit	[+35.39]	[−14.21]	[+2.86]	[−1.55]	[−0.03]	[−0.11]	[−0.01]	[+22.34]
$\Delta E = 22.34 - 3.57 - 0.06 + 0.01 = +18.73$ kcal mol^{-1}								
(d) $HBH(H_2)_2^+ \rightarrow C_s$ scrambling TS								
cc-pCVDZ	+15.12	−5.85	+0.88	−0.53	−0.04	−0.03	−0.00	[+9.54]
cc-pCVTZ	+15.39	−6.13	+1.06	−0.64	−0.02	−0.04	[−0.00]	[+9.63]
cc-pCVQZ	+15.42	−6.24	+1.10	−0.67	−0.01	[−0.04]	[−0.00]	[+9.56]
cc-pCV5Z	+15.42	−6.25	+1.10	−0.67	[−0.01]	[−0.04]	[−0.00]	[+9.55]
cc-pCV6Z	+15.42	−6.27	+1.10	−0.67	[−0.01]	[−0.04]	[−0.00]	[+9.53]
CBS limit	[+15.42]	[−6.29]	[+1.11]	[−0.68]	[−0.01]	[−0.04]	[−0.00]	[+9.51]
$\Delta E = 9.51 - 1.28 - 0.03 + 0.00 = +8.21$ kcal mol^{-1}								

[a]The symbol δ denotes the increment in the relative energy with respect to the preceding level of theory in the hierarchy HF→MP2→CCSD→CCSD(T)→CCSDT→CCSDT(Q)→CCSDTQ.
Square brackets signify results obtained from basis set extrapolations or additivity assumptions.
[b]Each final relative energy ΔE is the sum of ΔE_e[CCSDTQ/CBS], Δ_{ZPVE}[CCSD(T)/cc-pCVQZ], Δ_{DBOC}[CCSD/cc-pCVQZ], and Δ_{rel}[CCSD(T)/cc-pCVQZ], listed in order.

3 Vibrational Frequencies

3.1 CCSDTQ/CBS Geometries and Frequencies

As a gauge for estimating the quality of our CCSD(T)/cc-pCV5Z geometric parameters, we optimized the four smallest structures to the complete basis set (CBS) limit. This optimization was performed by the finite displacement of energy points using a 3-point formula, as generated by Psi4 and the Newton-Raphson approach. The absolute energy of each point was extrapolated to CCSDTQ/CBS via focal point analysis. The resulting optimized geometries for $B(H_2)^+$, $B(H_2)_2^+$, HBH^+ and $HBH(H_2)^+$ are shown in Figure S3, with cartesian coordinates listed in Table S14.

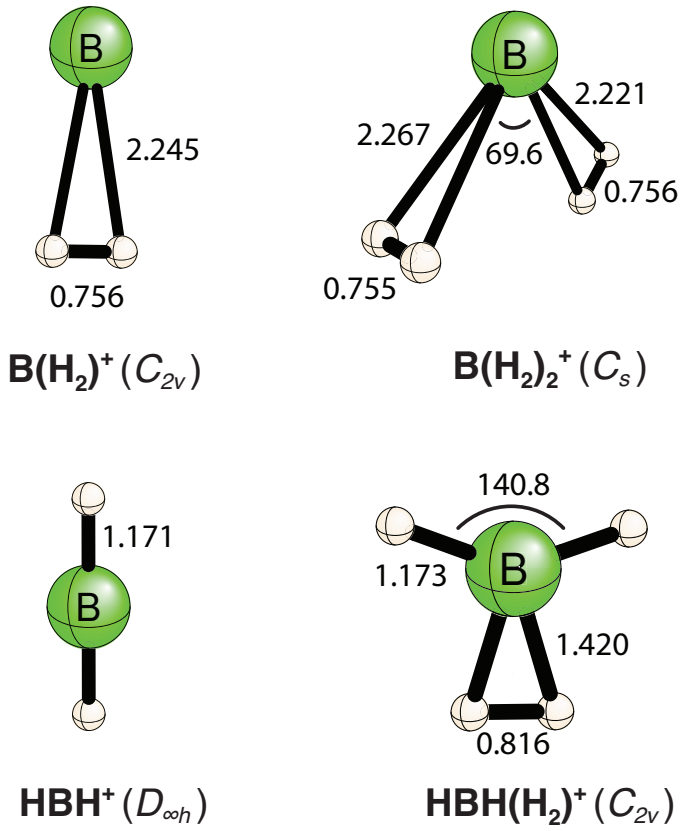

Figure S3: The optimized geometries (Å and degrees) of $B(H_2)^+$, $B(H_2)_2^+$, HBH^+, and $HBH(H_2)^+$ obtained at CCSDTQ/CBS level of theory.

Table S14: Cartesian coordinates (Å) optimized at CCSDTQ/CBS level of theory.

Atoms	X	Y	Z
(a) $B(H_2)^+$			
B	0.000 00	0.000 00	−0.342 45
H	0.000 00	−0.378 04	1.870 58
H	0.000 00	0.378 04	1.870 58
(b) $B(H_2)_2^+$			
B	0.428 36	0.164 55	0.000 00
H	−1.696 93	0.858 70	0.377 47
H	−1.696 93	0.858 70	−0.377 47
H	−0.306 98	−1.931 28	0.000 00
H	−0.978 67	−1.584 80	0.000 00
(c) HBH^+			
B	0.000 00	0.000 00	0.000 00
H	0.000 00	0.000 00	−1.170 48
H	0.000 00	0.000 00	1.170 48
(d) $HBH(H_2)^+$			
B	0.000 00	0.000 00	0.129 64
H	1.104 91	0.000 00	0.522 54
H	−1.104 91	0.000 00	0.522 54
H	−0.408 08	0.000 00	−1.230 66
H	0.408 08	0.000 00	−1.230 66

The harmonic frequencies of $B(H_2)^+$, $B(H_2)_2^+$, HBH^+, and $HBH(H_2)^+$, are calculated from the hessian matrices, evaluated numerically using a 3-point formula. Each energy point was extrapolated to the CCSDTQ/CBS level. The results are shown in Table S15–S17.

Table S15: Harmonic vibrational frequencies (cm^{-1}) of $B(H_2)_2^+$ computed at the CCSDTQ/CBS level of theory.

Symmetry	Modes	Harmonic
a'	ω_1	4214
	ω_2	4200
	ω_3	539
	ω_4	407
	ω_5	342
	ω_6	238
a''	ω_7	509
	ω_8	152
	ω_9	17

Table S16: Harmonic vibrational frequencies (cm^{-1}) of HBH^+ computed at the CCSDTQ/CBS level of theory.

Symmetry	Modes	Harmonic
σ_g^+	ω_1	2689
σ_u^+	ω_2	2975
π_u	ω_3	1000
	ω_3	1000

Table S17: Harmonic vibrational frequencies (cm^{-1}) of $HBH(H_2)^+$ computed at the CCSDTQ/CBS level of theory.

Symmetry	Modes	Harmonic
a_1	ω_1	3490
	ω_2	2700
	ω_3	1257
	ω_4	985
a_2	ω_5	853
b_1	ω_6	2901
	ω_7	1661
	ω_8	934
b_2	ω_9	963

3.2 CCSD(T) Harmonic and Fundamental Vibrational Frequencies

Table S18: Harmonic and fundamental vibrational frequencies (cm^{-1}), as well as corresponding infrared intensities (in parenthesis, km mol^{-1}) of $B(H_2)^+$ computed at the CCSD(T)/cc-pCVQZ level of theory, as compared to previous experimental[a] values.

Symmetry	Modes	Harmonic	Fundamental	Poad et al.[a]
a_1	ν_1	4200 (282.5)	3952	3940
	ν_2	351 (85.1)	309	N/A
b_2	ν_3	517 (15.4)	442	N/A

[a]Experimental value from *J. Chem. Phys.* 2012, **137**, 124312.

Table S19: Harmonic vibrational frequencies (cm^{-1}) and corresponding infrared intensities (km mol^{-1}) of $B(H_2)_2^+$ computed at the CCSD(T)/cc-pCVQZ level of theory.

Symmetry	Modes	Harmonic	Intensities
a'	ω_1	4218	228.6
	ω_2	4205	224.0
	ω_3	520	6.8
	ω_4	341	68.2
	ω_5	323	56.1
	ω_6	208	7.6
a''	ω_7	499	14.5
	ω_8	150	0.1
	ω_9	33	0.4

Table S20: Harmonic vibrational frequencies (cm^{-1}) and corresponding infrared intensities (km mol^{-1}) of $B(H_2)_3^+$ computed at the CCSD(T)/cc-pCVQZ level of theory.

Symmetry	Modes	Harmonic	Intensities
a	ω_1	4214	204.5
	ω_2	513	2.9
	ω_3	325	53.3
	ω_4	231	22.7
	ω_5	200	0.0
e	ω_6	4214	179.3
	ω_7	4214	179.3
	ω_8	504	8.5
	ω_9	504	8.5
	ω_{10}	317	40.5
	ω_{11}	317	40.5
	ω_{12}	211	2.5
	ω_{13}	211	2.5
	ω_{14}	115	0.4
	ω_{15}	115	0.4

Table S21: Harmonic and fundamental vibrational frequencies (cm^{-1}) and corresponding infrared intensities (km mol^{-1}) of HBH^+ computed using VPT2 method at the CCSD(T)/cc-pCVQZ level of theory.

Symmetry	Modes	Harmonic	Intensities	Fundamental	Intensities
σ_g^+	ω_1	2690	0.0	2601	0.0
σ_u^+	ω_2	2976	98.6	2865	99.9
π_u	ω_3	998	4.4	989	2.8
	ω_3	998	4.4	989	2.8

Table S22: Harmonic vibrational frequencies (cm^{-1}) and corresponding infrared intensities (km mol^{-1}) of $HBH(H_2)^+$ computed at the CCSD(T)/cc-pCVQZ level of theory.

Symmetry	Modes	Harmonic	Intensities
a_1	ω_1	3503	52.5
	ω_2	2703	9.2
	ω_3	1254	6.5
	ω_4	982	3.2
a_2	ω_5	847	0.0
b_1	ω_6	2903	50.9
	ω_7	1652	52.3
	ω_8	935	28.3
b_2	ω_9	966	0.0

Table S23: Harmonic vibrational frequencies (cm^{-1}) and corresponding infrared intensities (km mol^{-1}) of $HBH(H_2)_2^+$ computed at the CCSD(T)/cc-pCVQZ level of theory.

Symmetry	Modes	Harmonic	Intensities
a_1	ω_1	3430	1.9
	ω_2	2660	21.8
	ω_3	1321	17.8
	ω_4	1075	0.0
	ω_5	830	65.2
a_2	ω_6	1830	0.0
	ω_7	1066	0.0
	ω_8	665	0.0
b_1	ω_9	2781	54.5
	ω_{10}	1867	117.1
	ω_{11}	907	54.7
	ω_{12}	529	65.1
b_2	ω_{13}	3369	52.4
	ω_{14}	1302	13.8
	ω_{15}	1058	2.4

Table S24: Harmonic vibrational frequencies (cm^{-1}) and corresponding infrared intensities (km mol^{-1}) of the C_{2v} transition state for $B(H_2)_2^+ \rightarrow HBH(H_2)^+$ computed at the CCSD(T)/cc-pCVQZ level of theory.

Symmetry	Modes	Harmonic	Intensities
a_1	ω_1	$1192i$	59.3
	ω_2	2263	47.5
	ω_3	1516	14.4
	ω_4	793	29.8
a_2	ω_5	1011	0.0
b_1	ω_6	888	0.2
b_2	ω_7	2711	14.6
	ω_8	1684	57.7
	ω_9	1160	53.0

Table S25: Harmonic vibrational frequencies (cm^{-1}) and corresponding infrared intensities (km mol^{-1}) of the C_{3v} transition state for $B(H_2)_3^+ \rightarrow HBH(H_2)_2^+$ computed at the CCSD(T)/cc-pCVQZ level of theory.

Symmetry	Modes	Harmonic	Intensities
a_1	ω_1	$506i$	75.2
	ω_2	3700	68.9
	ω_3	865	21.2
	ω_4	623	0.8
a_2	ω_5	359	0.0
e	ω_6	3797	130.2
	ω_7	3797	130.2
	ω_8	824	1.1
	ω_9	824	1.1
	ω_{10}	631	48.4
	ω_{11}	631	48.4
	ω_{12}	587	0.0
	ω_{13}	587	0.0
	ω_{14}	335	4.6
	ω_{15}	335	4.6

Table S26: Harmonic vibrational frequencies (cm^{-1}) and corresponding infrared intensities (km mol^{-1}) of the D_{3h} hydrogen scrambling transition state for $HBH(H_2)_2^+$ computed at the CCSD(T)/cc-pCVQZ level of theory.

Symmetry	Modes	Harmonic	Intensities
a_1'	ω_1	2325	0.0
	ω_2	1528	0.0
a_1''	ω_3	1225	0.0
a_2''	ω_4	2579	320.0
	ω_5	503	345.9
e'	ω_6	$1069i$	725.9
	ω_7	$1069i$	725.9
	ω_8	2592	129.5
	ω_9	2592	129.5
	ω_{10}	902	18.1
	ω_{11}	902	18.1
e''	ω_{12}	2479	0.0
	ω_{13}	2479	0.0
	ω_{14}	1041	0.0
	ω_{15}	1041	0.0

Table S27: Harmonic vibrational frequencies (cm^{-1}) and corresponding infrared intensities (km mol^{-1}) of the C_s hydrogen scrambling transition state for $HBH(H_2)_2^+$ computed at the CCSD(T)/cc-pCVQZ level of theory.

Symmetry	Modes	Harmonic	Intensities
a'	ω_1	3299	24.5
	ω_2	2836	48.6
	ω_3	2489	63.5
	ω_4	2342	28.0
	ω_5	1466	34.2
	ω_6	1366	11.0
	ω_7	1145	5.5
	ω_8	995	5.4
	ω_9	860	68.1
a''	ω_{10}	$1189i$	453.3
	ω_{11}	2420	52.9
	ω_{12}	1924	64.1
	ω_{13}	1159	4.7
	ω_{14}	954	3.7
	ω_{15}	564	77.6

4 Molecular Orbital Analysis

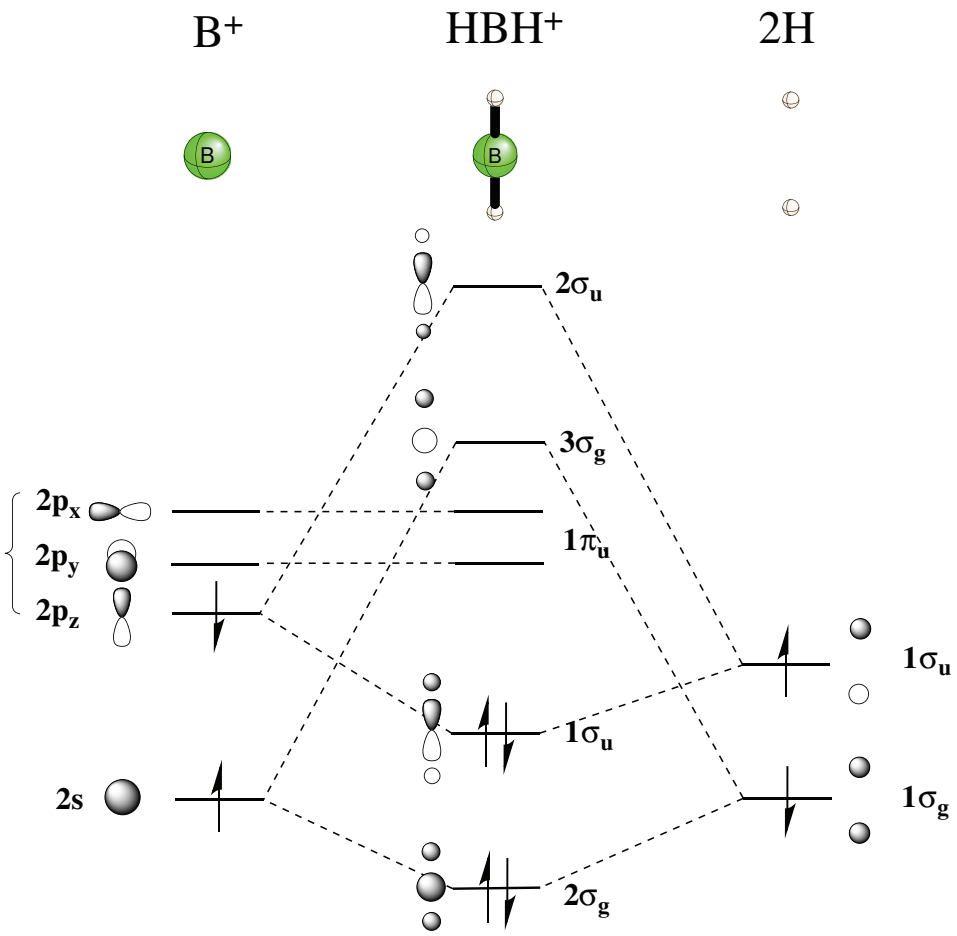

Figure S4: Orbital correlation diagram for the formation of HBH^+ from B^+ and two H fragments. The curly brace on the left indicates the degeneracy of B^+ $2p$ orbitals.

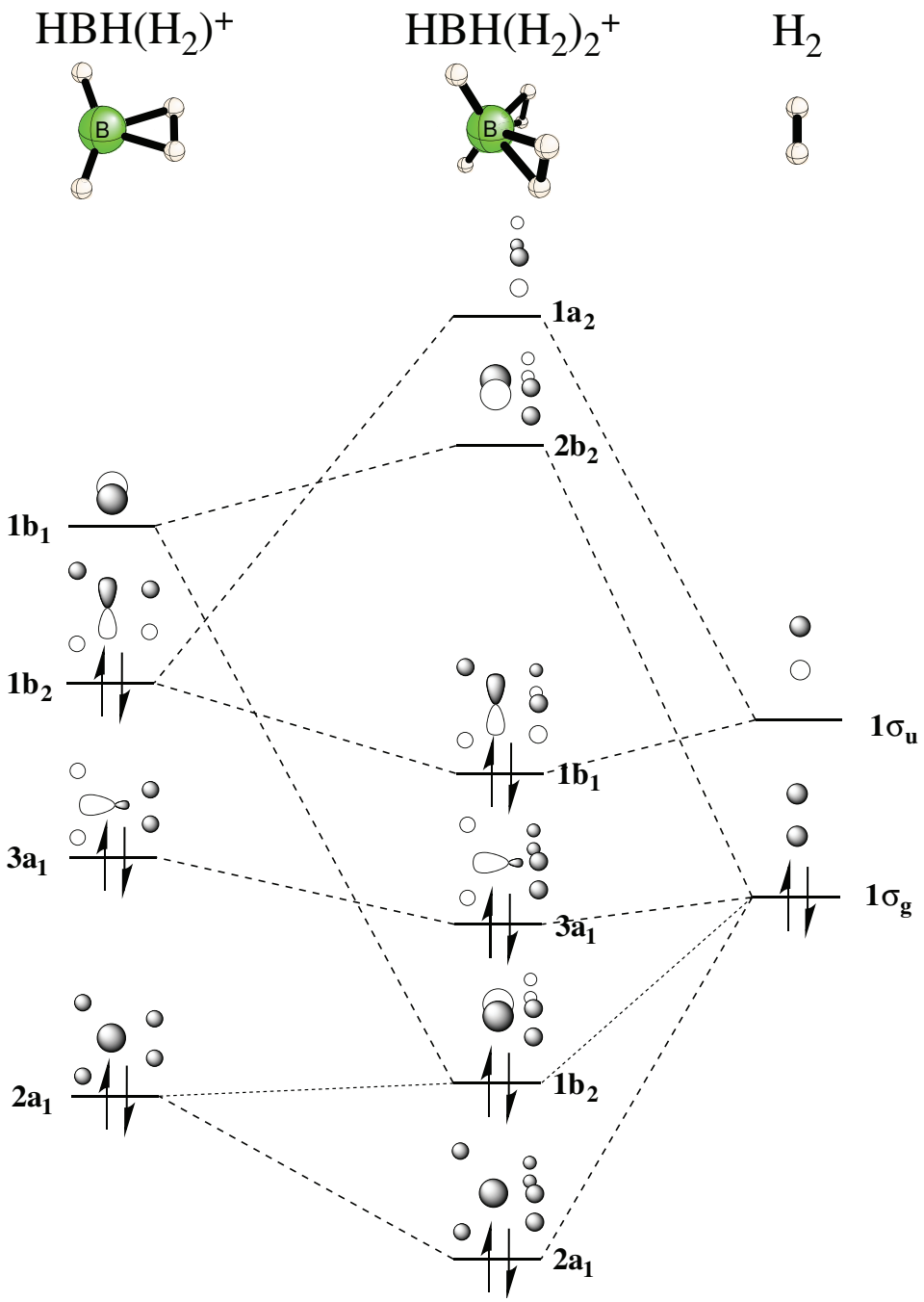

Figure S5: Oribital correlation diagram for the formation of $HBH(H_2)_2^+$ from $HBH(H_2)^+$ and H_2 fragments. Large contributions of fragment orbitals are indicated by the dashed lines, while small contributions are depicted by the dotted lines.

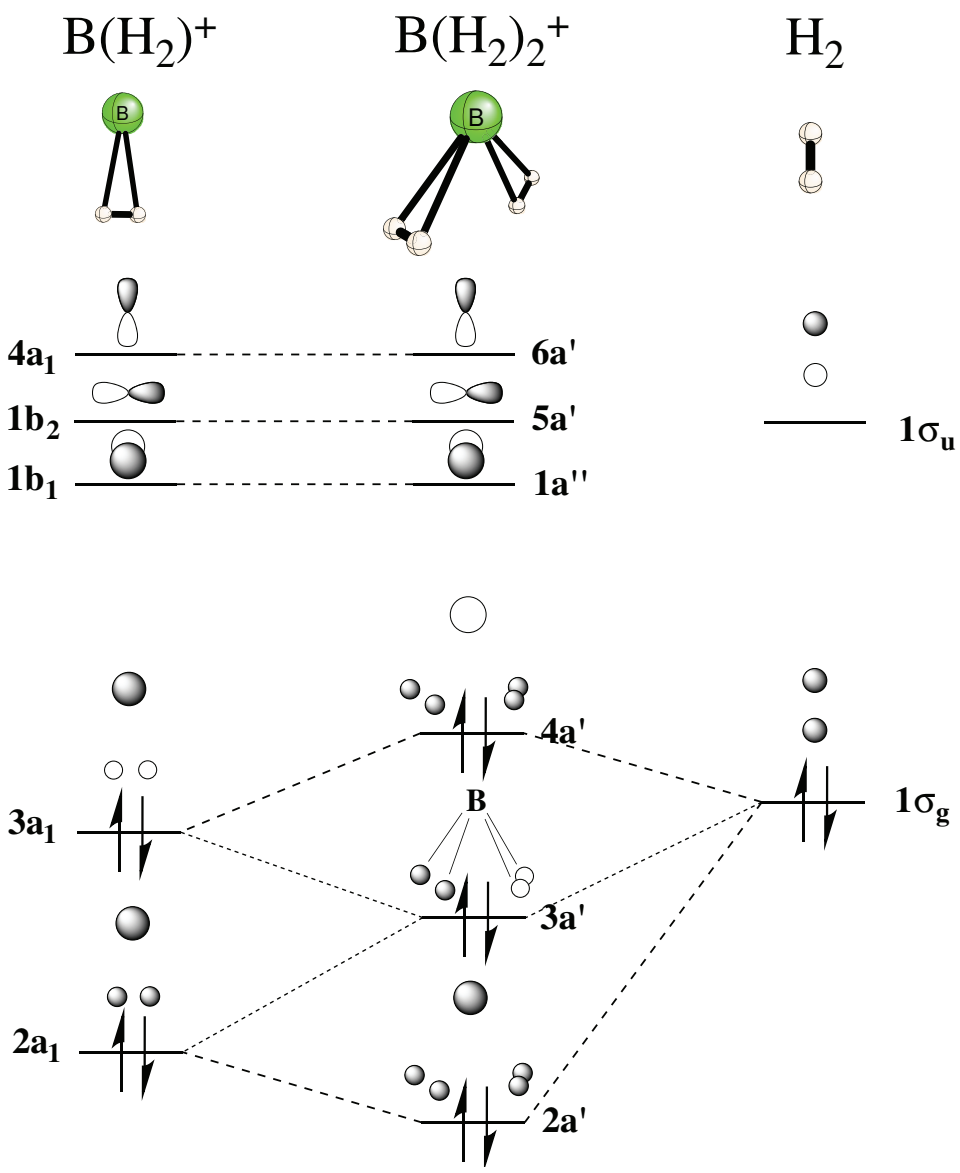

Figure S6: Oribital correlation diagram for the formation of $B(H_2)_2^+$ from $B(H_2)^+$ and H_2 fragments. Large contributions of fragment orbitals are indicated by the dashed lines, while small contributions are depicted by the dotted lines. The interaction between the 3a′ and 5a′ orbitals of $B(H_2)_2^+$ provides critical stabilization for the H–H σ bond activation process.

5 Intrinsic Reaction Coordinates

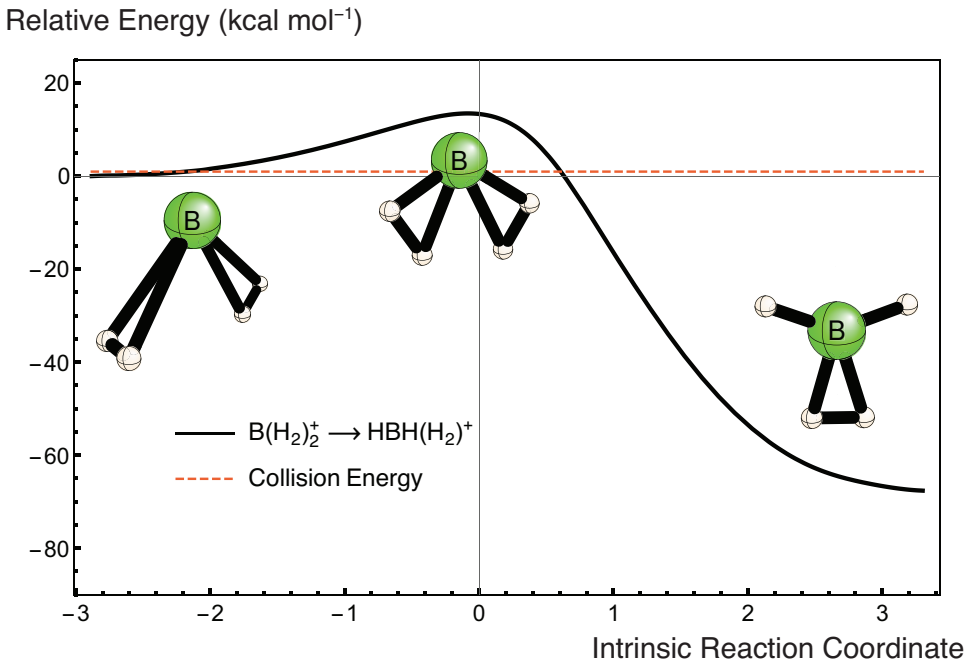

Figure S7: Complete potential energy curve along the intrinsic reaction path (IRP) for the insertion reaction of $B(H_2)_2^+$. The geometric structures and zero-point vibrational corrections along the path were generated at the AE-CCSD(T)/cc-pCVTZ level of theory. Final energetics were determined from AE-CCSD(T)/cc-pCV5Z single points along the IRP. The abscissa is the intrinsic reaction coordinate (in units of $u^{1/2}$ bohr) along the path in mass-weighted Cartesian coordinates.

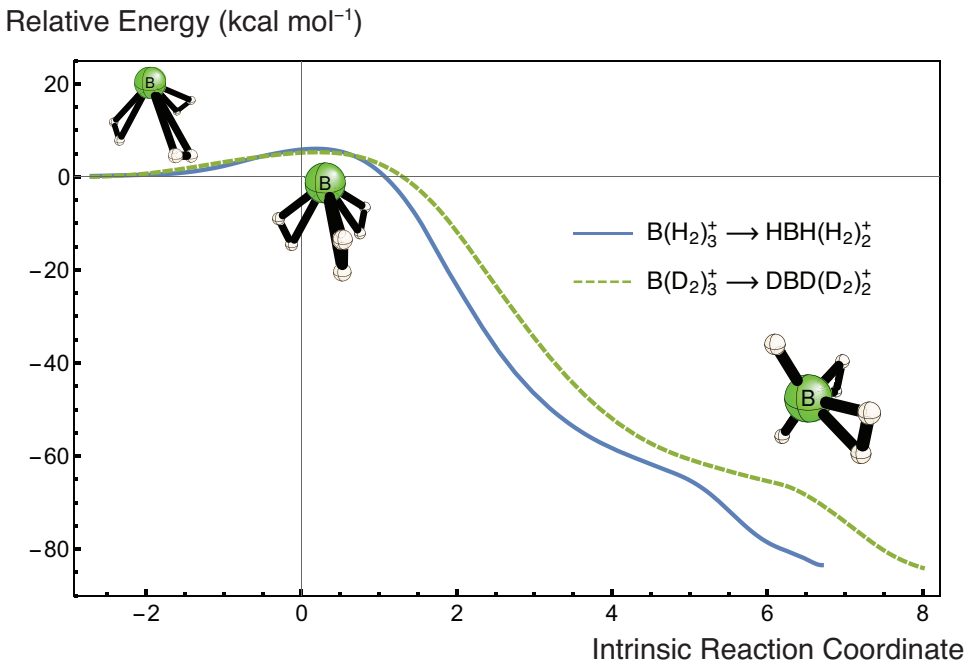

Figure S8: Complete potential energy curves along the intrinsic reaction path (IRP) for the indicated insertion reactions. The geometric structures and zero-point vibrational corrections along the path were generated at the AE-CCSD(T)/cc-pCVTZ level of theory. Final energetics were determined from AE-CCSD(T)/cc-pCV5Z single points along the IRP. The abscissa is the intrinsic reaction coordinate (in units of $u^{1/2}$ bohr) along the path in mass-weighted Cartesian coordinates. The shoulder in the product region is caused by disturbance from the H/D scrambling modes.

Table S28: Key parameters and results from the tunneling analysis using WKB and exact scattering methods for the insertion reactions $B(H_2)_3^+ \rightarrow HBH(H_2)_2^+$ and $B(D_2)_3^+ \rightarrow DBD(D_2)_2^+$.

$B(H_2)_3^+ \rightarrow HBH(H_2)_2^+$	$B(D_2)_3^+ \rightarrow DBD(D_2)_2^+$
(a) WKB	
Collision energy (ϵ) = 0.47 kcal mol^{-1}	Collision energy (ϵ) = 0.37 kcal mol^{-1}
Collision frequency (ω_0) = 332 cm^{-1}	Collision frequency (ω_0) = 261 cm^{-1}
Barrier = 6.07 kcal mol^{-1}	Barrier = 5.10 kcal mol^{-1}
Turning points (s1, s2) = (−2.00, 1.05) u$^{1/2}$ bohr	Turning points (s1, s2) = (−2.52, 1.24) u$^{1/2}$ bohr
Effective barrier frequency = 658i cm^{-1}	Effective barrier frequency = 397i cm^{-1}
Barrier penetration integral (θ) = 11.47	Barrier penetration integral (θ) = 13.52
Transmission probability (P_H) = 1.10×10^{-10}	Transmission probability (P_D) = 1.80×10^{-12}
Pure Tunneling half-life (τ) = 6.34×10^{-4} s	Pure Tunneling half-life (τ) = 4.91×10^{-2} s
(b) Exact Scattering	
Transmission probability (P_H) = 8.54×10^{-11}	Transmission probability (P_D) = 1.59×10^{-12}
Pure Tunneling half-life (τ) = 8.16×10^{-4} s	Pure Tunneling half-life (τ) = 5.56×10^{-2} s

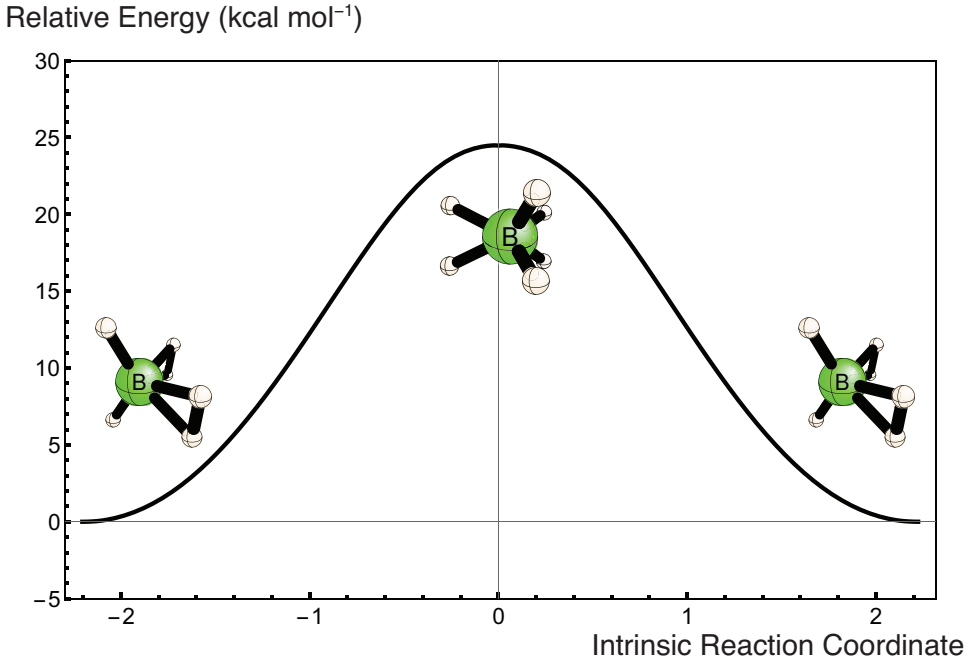

Figure S9: Intrinsic reaction path (IRP) for the hydrogen scrambling reaction of $HBH(H_2)_2^+$ through the D_{3h} transition state, computed at AE-CCSD/cc-pCVTZ level. The abscissa is the intrinsic reaction coordinate (in units of u$^{1/2}$ bohr) along the path in mass-weighted Cartesian coordinates.

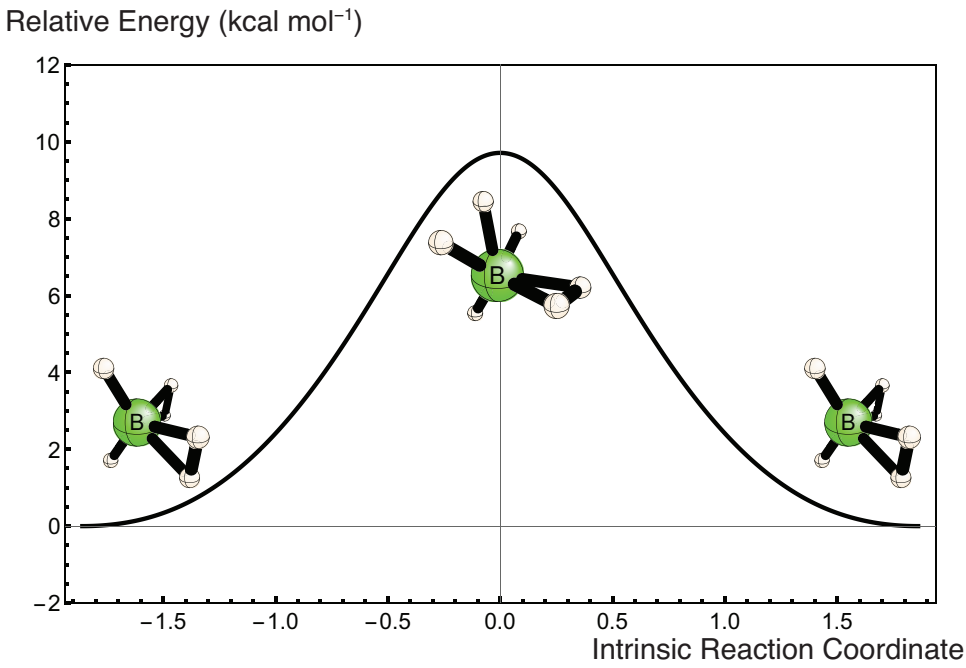

Figure S10: Intrinsic reaction path (IRP) for the hydrogen scrambling reaction of $HBH(H_2)_2^+$ through the C_s transition state, computed at AE-CCSD/cc-pCVTZ level. The abscissa is the intrinsic reaction coordinate (in units of $u^{1/2}$ bohr) along the path in mass-weighted Cartesian coordinates.

6 Tunneling Analyses

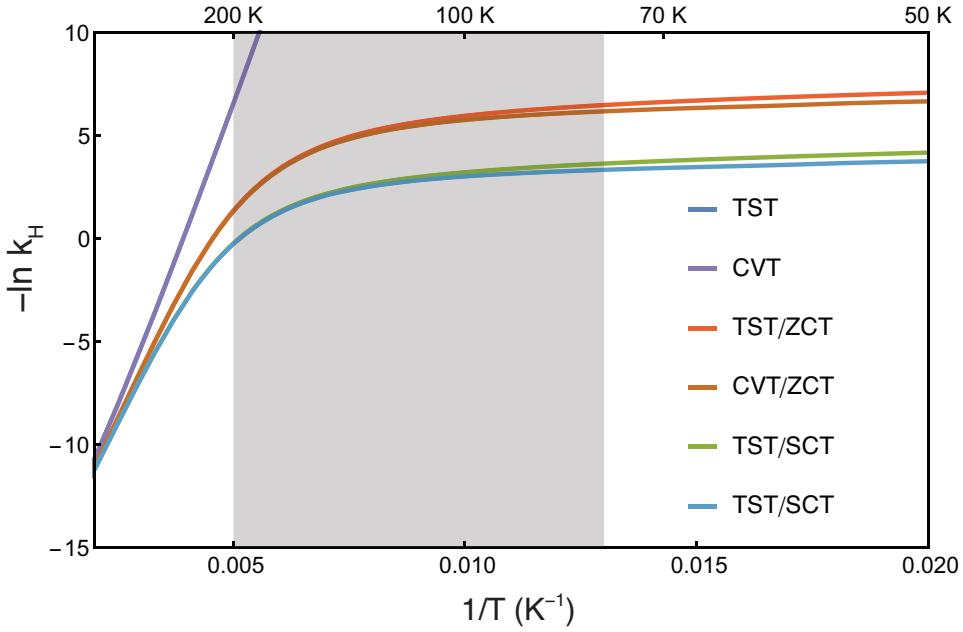

Figure S11: Arrhenius plot of rate constants for the insertion reaction $B(H_2)_2^+ \rightarrow HBH(H_2)^+$, obtained by conventional transition state theory (TST) or canonical variational transition state theory (CVT), each with zero-curvature tunneling (ZCT) and small-curvature tunneling (SCT). The grey area indicates the experimental temperature range of the overall insertion reaction rate.

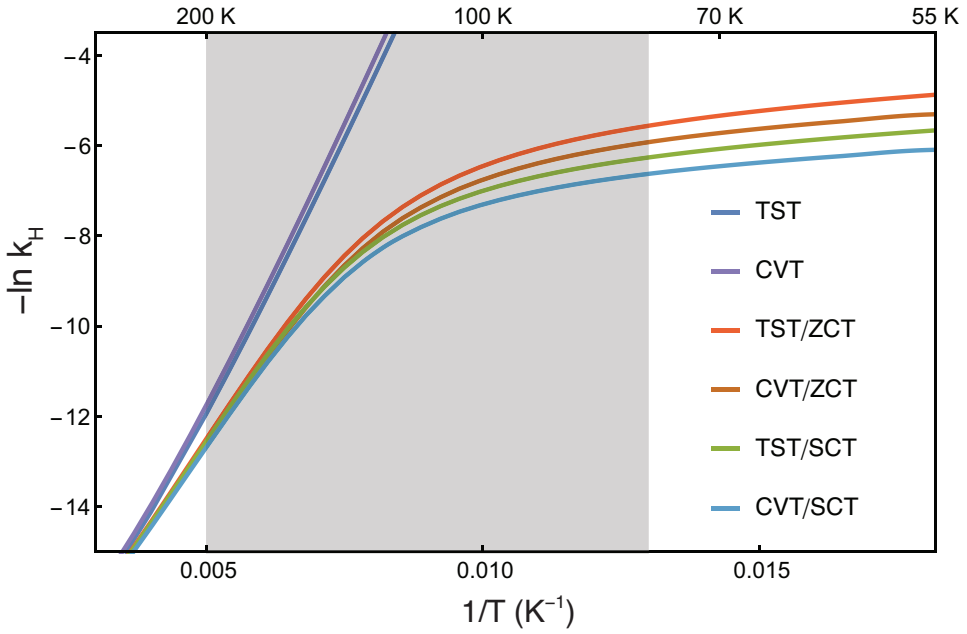

Figure S12: Arrhenius plot for the insertion reaction $B(H_2)_3^+ \rightarrow HBH(H_2)_2^+$, obtained by conventional transition state theory (TST) or canonical variational transition state theory (CVT), each with zero-curvature tunneling (ZCT) and small-curvature tunneling (SCT). The grey area indicates the experimental temperature range of the overall insertion reaction rate.

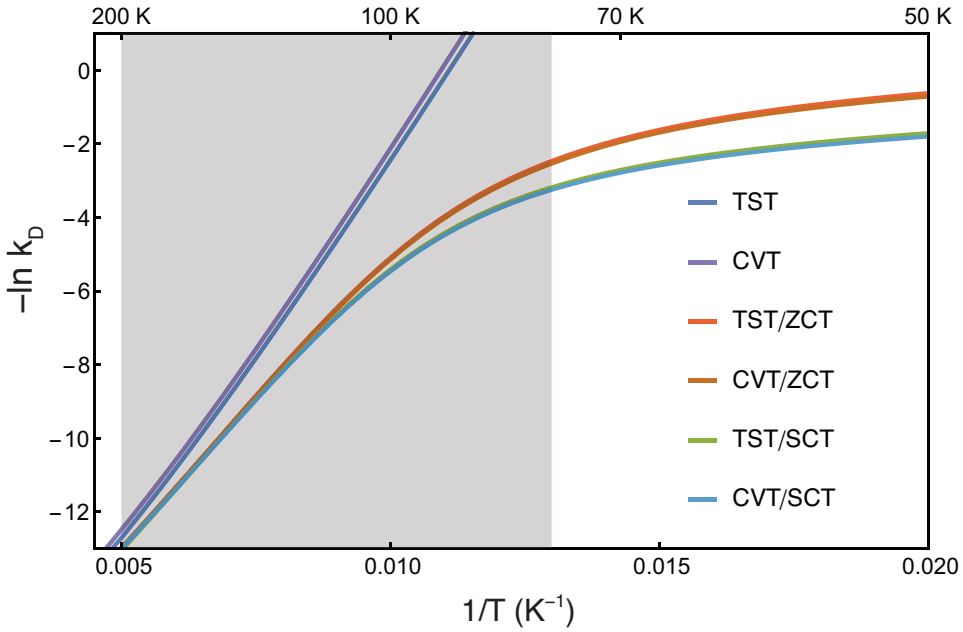

Figure S13: Arrhenius plot for the insertion reaction $B(D_2)_3^+ \rightarrow DBD(D_2)_2^+$, obtained by conventional transition state theory (TST) or canonical variational transition state theory (CVT), each with zero-curvature tunneling (ZCT) and small-curvature tunneling (SCT). The grey area indicates the experimental temperature range of the overall insertion reaction rate.

7 Estimation of $[B(H_2)_3^+]/[B(H_2)_2^+]$ Ratio under Experimental Conditions

Considering the experimental environment of Kemper and coworkers' rate constant measurements (Fig. 6 in Kemper, P. R.; Bushnell, J. E.; Weis, P.; Bowers, M. T. *J. Am. Chem. Soc.* 1998, 120, 7577–7584.), the temperature range is 75 K – 200 K, and the H_2 pressure = 2 torr = 0.0026 atm.

Based on the data in Table 1 of this paper, we assume for the binding reactions $B(H_2)_{n-1}^+ + H_2 \rightarrow B(H_2)_n^+$ the entropy change $\Delta S \approx 14$ cal mol^{-1} K^{-1}. Taking the experimental enthalpy change $\Delta H = -3.4$ kcal mol^{-1} for $B(H_2)^+ + H_2 \rightarrow B(H_2)_2^+$, appended by our computed binding energy difference between $B(H_2)_2^+$ and $B(H_2)_3^+$ ($2.9 - 2.5 = 0.4$ kcal mol^{-1}), we estimate the enthalpy change for binding reaction $B(H_2)_2^+ + H_2 \rightarrow B(H_2)_3^+$ as

$$\Delta H = -3.4 + 0.4 = -3.0 \text{ kcal mol}^{-1} \quad , n = 3 \tag{1}$$

For each temperature T, we estimate the Gibbs free energy change using

$$\Delta G_T = \Delta H - T\Delta S \tag{2}$$

Then, based on the fact that rapid equilibrium was established between all reactants $B(H_2)_n^+$, the $[B(H_2)_3^+]/[B(H_2)_2^+]$ ratio is obtained by the following relations:

$$\Delta G_T = -RT \ln K_{eq} \tag{3}$$

$$\ln K_{eq} = \frac{[B(H_2)_3^+]}{[B(H_2)_2^+][H_2]} \tag{4}$$

The results are shown in Table S29. Our estimation shows the $[B(H_2)_3^+]/[B(H_2)_2^+]$ ratio is larger than 0.004 in the experimental temperature range. Even if our estimated ΔG has

an error of 0.5 kcal mol^{-1}, the $[B(H_2)_3^+]/[B(H_2)_2^+]$ ratio still remains larger than 0.001.

Table S29: Estimation of $[B(H_2)_3^+]/[B(H_2)_2^+]$ Ratio Under Experimental Conditions

Temperature (K)	ΔG_T (kcal mol^{-1})	$[B(H_2)_3^+]/[B(H_2)_2^+]$
70	−2.02	5330
80	−1.88	360
90	−1.74	44.2
100	−1.60	8.26
110	−1.46	2.09
120	−1.32	0.667
130	−1.18	0.253
140	−1.04	0.111
150	−0.90	0.0539
160	−0.76	0.0287
170	−0.62	0.0165
180	−0.48	0.0101
190	−0.34	0.00648
200	−0.20	0.00435

8 Details for the Active Space of BH_2^+ PES

As shown in Table S30, the leading CI coefficients from all-electron/full-valence CAS(6,7) computations indicate that the single-reference reactant $B(H_2)^+$ (S = −5) gradually converted into the two-configurational TS (S = 0), then further merged to the single-reference product HBH^+ (S = +2). Therefore, a CAS(2,2) reference including the two active orbitals from the open-shell singlet TS is sufficient to describe the PES of BH_2^+ in an Mk-MRCCSD(T) computation.

Table S30: Leading CI coefficients (C_i) in the CASPT2/cc-pCVQZ wave functions along the $B(H_2)^+ \rightarrow HBH^+$ Intrinsic Reaction Path[a]

	CAS(6,7)			
S[a] ($u^{1/2}$ bohr)	C_1	C_2	C_3	C_4
−5.82	0.95	−0.17	−0.17	−0.15
−5.14	0.95	−0.17	−0.17	−0.15
−4.75	0.95	−0.17	−0.17	−0.15
−4.14	0.95	−0.17	−0.17	−0.14
−3.77	0.95	−0.17	−0.17	−0.14
−3.14	0.93	−0.20	−0.15	−0.15
−2.42	0.89	−0.37	−0.08	−0.08
−1.80	0.84	−0.50	−0.06	−0.06
−1.40	0.81	−0.55	−0.06	−0.06
−0.99	0.77	−0.62	−0.06	−0.06
−0.56	0.75	−0.64	−0.06	−0.06
−0.22	0.73	−0.66	−0.06	−0.06
+0.00	0.71	−0.68	−0.06	−0.06
+0.23	0.72	−0.68	−0.06	−0.06
+0.53	0.80	−0.58	−0.06	−0.06
+0.99	0.94	−0.30	−0.08	−0.07
+1.46	0.98	−0.10	−0.08	−0.07
+1.76	0.99	−0.07	−0.07	−0.06

[a]S is the intrinsic reaction coordinate (in units of $u^{1/2}$ bohr) along the path in mass-weighted Cartesian coordinates

9 Example Keywords and Parameters in Polyrate Computations

Table S31: Example keywords and parameters in Polyrate computations.

poly.fu5		poly.fu40	
*PATH		*gen40	
NSTEPS	500	curvature	compute
COORD	cart	gradder	noextra
RPM	ESD	freqsource	hessian
INH	1	hessform	full
SADDLE	yes	anharm	none
HESS	off	maxlpts	3
SSTEP	0.03		
CURV	dgrad		
FIRSTSTEP	nmode		
SIGN	reactant		